ELSEVIER

Journal of Alloys and Compounds 444–445 (2007) 217–225

Journal of ALLOYS AND COMPOUNDS

www.elsevier.com/locate/jallcom

X-ray diffraction analyses of aged U–Nb alloys

H.M. Volz *, R.E. Hackenberg, A.M. Kelly, W.L. Hults, A.C. Lawson, R.D. Field, D.F. Teter, D.J. Thoma

Los Alamos National Laboratory, Los Alamos, NM 87545, United States

Received 31 August 2006; received in revised form 15 November 2006; accepted 16 November 2006
Available online 28 December 2006

Abstract

An aging study of compositionally homogeneous U–5.6Nb and U–7.7Nb (wt.%) was undertaken to improve the understanding of the decomposition of metastable martensitic phases in the U–Nb system. Artificially aging these depleted (^{238}U) uranium alloys at 373, 473, 523 and 573 K for times up to 70 days resulted in significant age hardening. However, the microstructural changes giving rise to this hardening are subtle and elude standard light optical and electron microscopy techniques; this subtlety motivated the present study of aging-related changes by X-ray diffraction. A sealed tube X-ray diffractometer was used to record powder diffraction patterns from these aged polycrystalline U–Nb samples along with a CeO_2 standard. Data were analyzed using GSAS for full-pattern Rietveld refinements. Planar defects as well as strain broadening appear to have caused unusual peak profiles, which makes data interpretation challenging. Lattice parameter and unit cell volume trends are presented. U–5.6Nb experienced a reversal in the *b* lattice parameter and unit cell volume during aging, which has both similarities and differences to aging in dilute U–Ti and U–Mo alloys. The longest-time aging unit cell volume trends of U–5.6Nb indicate Nb depletion of the matrix phase, while the corresponding behavior at all aging times in U–7.7Nb is indicative of Nb enrichment in its matrix phase.

Keywords: Uranium; Alloy; Diffraction; Lattice parameter changes

1. Introduction

Uranium and its alloys are employed in various applications due to their high density and nuclear properties. Alloying uranium with certain transition metals such as niobium improves corrosion resistance and allows tailoring of mechanical properties including strength and ductility. At equilibrium over a wide range of U–Nb alloy compositions at room temperature, a two phase mixture of orthorhombic α-uranium and body-centered cubic (bcc) γ phase is expected (Fig. 1) [1,4,11]. This equilibrium phase mixture has poor corrosion and mechanical properties; therefore the material is typically quenched from the γ phase to retain Nb in metastable martensitic phases that show improved corrosion resistance and high ductility. Fig. 1 shows the metastability ranges of these martensitically formed phases. Orthorhombic α′ and monoclinic α″ are both distorted forms of the orthorhombic α-uranium phase in pure uranium, while the tetragonal phase γ^0 is a variant of γ with the atoms slightly displaced from their ideal bcc positions.

Although prior work involved understanding processing steps necessary to create specific metastable phases [2], little is known about the long-term phase stability of these alloys, particularly the mechanism and path by which they transform to the eventual equilibrium state at temperatures less than 623 K. This paper reports on the changes in mechanical properties, lattice parameters of the phases, and microstructures in compositionally homogeneous U–Nb model alloys aged at 573 K and below. The lack of visible microstructural changes stands in contrast with the significant mechanical property changes from aging. Hence, this study emphasizes X-ray diffraction as a characterization technique, since lattice parameter changes appear to be more sensitive to aging than any visible microstructural changes in these alloys.

Lattice parameter studies of uranium alloys from the literature show decreasing unit cell volume with increasing niobium concentration across all the metastable phases listed in Fig. 1, consistent with a smaller substitutional atom [3–5]. The effect is highly anisotropic, with *b* lattice parameter sharply decreasing with increasing niobium concentration. As aging progresses we expect the system to equilibrate with two phases: a pure α-U matrix and Nb-rich γ phase precipitates. Therefore, based on

* Corresponding author. Tel.: +1 505 665 4370; fax: +1 505 667 5268.
E-mail address: hvolz@lanl.gov (H.M. Volz).

0925-8388/$ – see front matter © 2006 Elsevier B.V. All rights reserved.
doi:10.1016/j.jallcom.2006.11.089

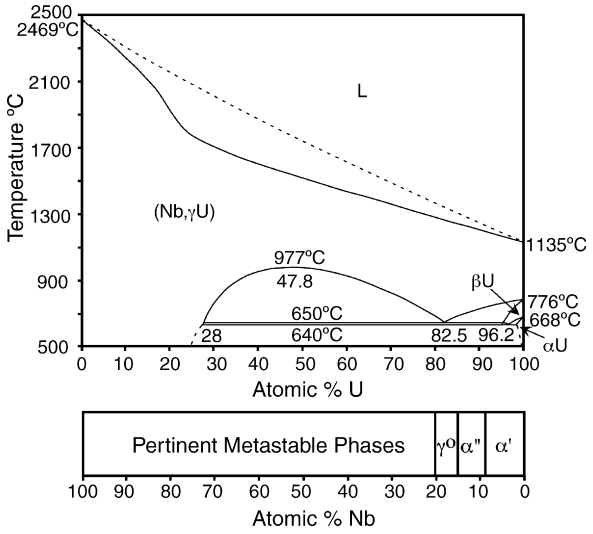

Fig. 1. U–Nb binary phase diagram, adapted from Refs. [1,4]. The equilibrium phases in the aging regime of interest are almost pure orthorhombic α-U and body-centered cubic γ containing ∼54 wt.% (∼75 at.%) Nb. The martensitic phases retained after quenching from γ solutionizing temperatures are monoclinic α″ in U–5.6 wt.% (13.2 at.%) Nb and tetragonal γ^0 in U–7.7 wt.% (17.6 at.%) Nb [11].

the literature and assuming Nb diffuses out of solution to feed Nb-rich precipitate formation, we would expect the unit cell volume of matrix U-rich martensitic α″ to increase. Conversely, if a Nb-lean α-like phase were to form in the U–7.7Nb alloy (γ^0 matrix), this matrix phase would be enriched in niobium and increase the unit cell volume.

2. Experimental

U–Nb alloys were induction melted and cast into 0.5 in. thick plates, then hot rolled 50% and held at 1273 K for 6 h to produce compositionally homogenous plate. Compositions selected for study were U–5.6Nb and U–7.7Nb (values from wet chemical analysis; all compositions are reported in weight percent unless otherwise indicated; all samples depleted uranium, ^{238}U, $t_{1/2}$ of 4.5×10^9 years such that radiation damage within the timeframe of this experiment is considered negligible). Coupons and tensile specimens were solutionized in the γ (bcc) phase at 1073 K (U–5.6Nb) or 1123 K (U–7.7Nb) for 30 min and water quenched to form the α″ (U–5.6Nb) or γ^0 (U–7.7Nb) niobium-supersaturated martensitic phases, and samples from this step were retained as controls. The remaining samples were artificially aged via heat treatments in vacuum encapsulations. Five samples each were placed in furnaces at 373, 473, 523, and 573 K (20 aging samples total per composition). One sample from each furnace was removed at 10, 100, 1000, 10,000, and 100,000 min, although a few samples strayed from this schedule for logistical reasons. Note that these data were from separate samples, not from one thermally cycled sample.

All data presented in this study were collected at room temperature; changes in lattice parameters will not be due to thermal expansion effects.

Light optical micrographs were taken on coupons that were epoxy mounted and cured without any additional external heating. They were mechanically ground and polished down to 1 μm diamond. Samples were subsequently electrolytically etched 2–3 s at 3–4 V with 5% phosphoric acid, then 3–5 s at 4–5 V with 10% oxalic acid [6,7].

Specimens for transmission electron microscopy (TEM) were prepared from 3 mm diameter discs punched out of slices cut from the coupons and mechanically thinned. The discs were twin-jet electrolytically etched at 25 V and approximately −10 °C in a methanol solution containing 6% perchloric acid and 35% butyl 2-ethoxyethanol. They were examined in TEM instruments operating at 300 kV.

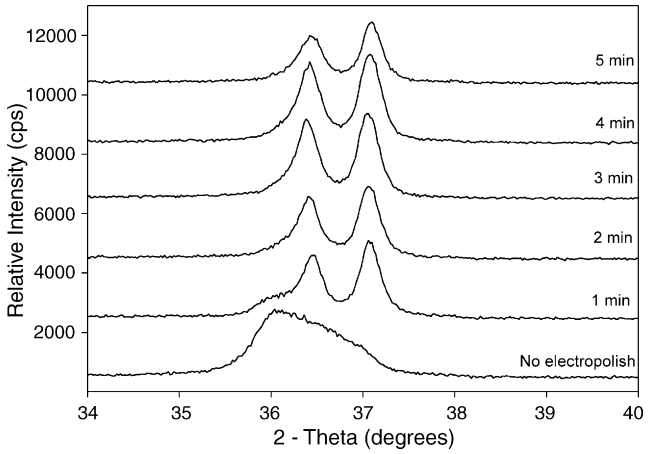

Fig. 2. Change in appearance of X-ray diffraction data with electrolytic etch time for as-quenched U–7.7Nb. Three minutes was found to be optimal for this sample, and was subsequently used for all aged samples. Intensities have been staggered for easier viewing.

Tensile testing was done on a screw driven machine at a strain rate of 0.001 s^{-1}. Strain was measured with an extensometer. Any visible oxide scale on the tensile specimens after aging was removed prior to testing by intermittent electrolytic etching at 12 V in a solution of 85% phosphoric acid, 2% sulfuric acid, and 13% water.

For a high atomic number element, the X-ray penetration depth for Cu Kα radiation is only 1–2 μm, and an oxide layer typically forms on these alloys within a week. Therefore, surface preparation was an important consideration in this study, and was optimized prior to data collection. Samples were mounted in epoxy and mechanically polished to a 1 μm diamond finish. An electrolytic etch solution was selected containing 35% H_2O, 60% H_3PO_4, and 5% H_2SO_4 [6,7], with an applied 12 V at room temperature. The change in appearance of X-ray diffraction peaks with varying amounts of etch time was examined, with 3 min selected based on peak-to-trough intensity ratios (Fig. 2).

A Bruker D8 Advance laboratory X-ray powder diffractometer was used in Bragg–Brentano geometry. The sealed Cu Kα tube was set to 40 kV and 40 mA, Soller slits were positioned at the tube exit [8], and the detector was a scintillation counter with a graphite diffracted beam monochromator. A sample stage motor spun the samples during data collection, thereby improving the randomization of the grain orientations in the large-grained polycrystalline specimens (50–150 μm prior γ grains observed microscopically, though the martensitic twins were submicron in scale). Data were collected from 20° to 148° in 2θ with wide divergence and anti-scattering slits and long count times, requiring 22 h per data set to achieve acceptable counting statistics from large-grained samples exhibiting significant peak broadening. Ceria powder (NIST SRM 674 a) was applied to a thin layer of vacuum grease on the metallographic mount around the sample for improved accuracy of the sample displacement correction [9], although a moderately aged U–5.6Nb sample was re-run with a LaB_6 powder standard (NIST SRM 660a) to ensure that the presence of CeO_2 was not masking any oxide phase.

GSAS was used to analyze data via full-pattern Rietveld refinement [10]. During the Rietveld refinements, atom positions were checked to make sure they were not drifting away from accepted values, and the isotropic thermal motion parameter (Uiso) for the heavily aged U–7.7Nb data and all of the U–5.6Nb data sets had to be fixed at a realistic value due to its tendency to become unrealistically negative. Fractional occupancies of atomic positions could not be successfully refined. Data were analyzed with several slightly different methodologies in order to confirm these trends and to seek the best fits to the data (LeBail versus Rietveld; different pseudo-Voigt peak profile choices for strain broadening and peak asymmetries). We selected a refinement strategy based on the best graphical fit of the Rietveld refinement to the data, plus a realistic selection of refinement variables and their final values. Once chosen, the same refinement strategy was used for all data of that composition, except for the most challenging refinements of the heavily aged specimens in which certain additional variables had to be fixed. Refinement specifics are discussed in more detail in Section 3.

Atypical behavior was observed in many of the data sets as the least-squares algorithm compromised on finding suitable peak positions. For example, low- and high-angle data in certain diffraction patterns showed a tendency to refine to a larger lattice parameter, but the mid-range data showed the opposite trend towards smaller values. This could not be accounted for by instrument parameters, but may be indicating another phenomenon. Planar faults (i.e., stacking faults, twin boundaries, coherency strain at phase boundaries) may have an important influence on all of the diffraction patterns, and will be pursued in future studies to determine if superior fits to the data are realized by accounting for these microstructural features [11].

3. Results and discussion

Figs. 3 and 4 show the effect of aging on the hardness and tensile response of both alloys. An age hardening response is observed for the times and temperatures examined: the hardness, yield strength, and tensile strength increase, and the tensile elongation decreases with aging time. The rates of these property changes increase with increasing temperature, consistent with a thermally activated mechanism, perhaps controlled by diffusion of Nb in the matrix, as was shown for U–4.5Nb [12]. Figs. 5 and 6 show light optical microstructures in as-quenched and heavily aged conditions. The bright field illumination in Figs. 5a and 6a highlights the prior γ grain structure as well as UC and Nb_2C inclusion distribution in the as-quenched conditions, while the differential interference contrast illumination in Figs. 5b and 6b highlight the martensitic twin structure and lack of any coarse-scale aging-related microstructural changes after significant aging, such as grain-boundary-initiated cellular decomposition which has been observed at >623 K in U–Nb and in other uranium alloys [12,13].

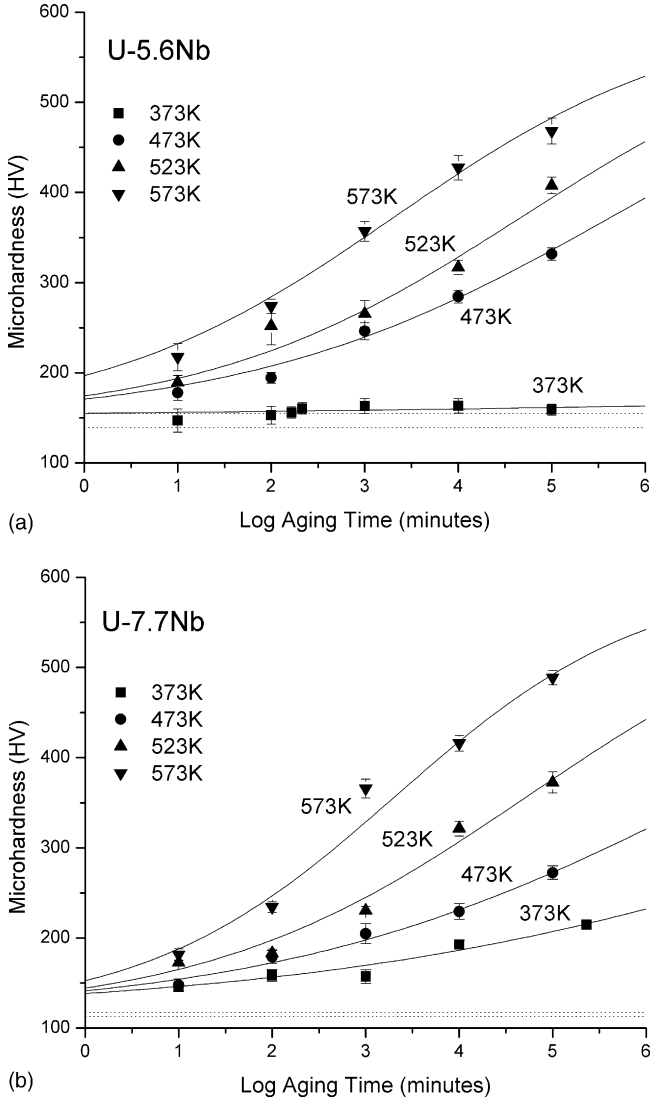

Fig. 3. Vickers microhardness response after aging for (a) U–5.6Nb and (b) U–7.7Nb. Dotted lines indicate the as-quenched hardness value ±1 standard deviation.

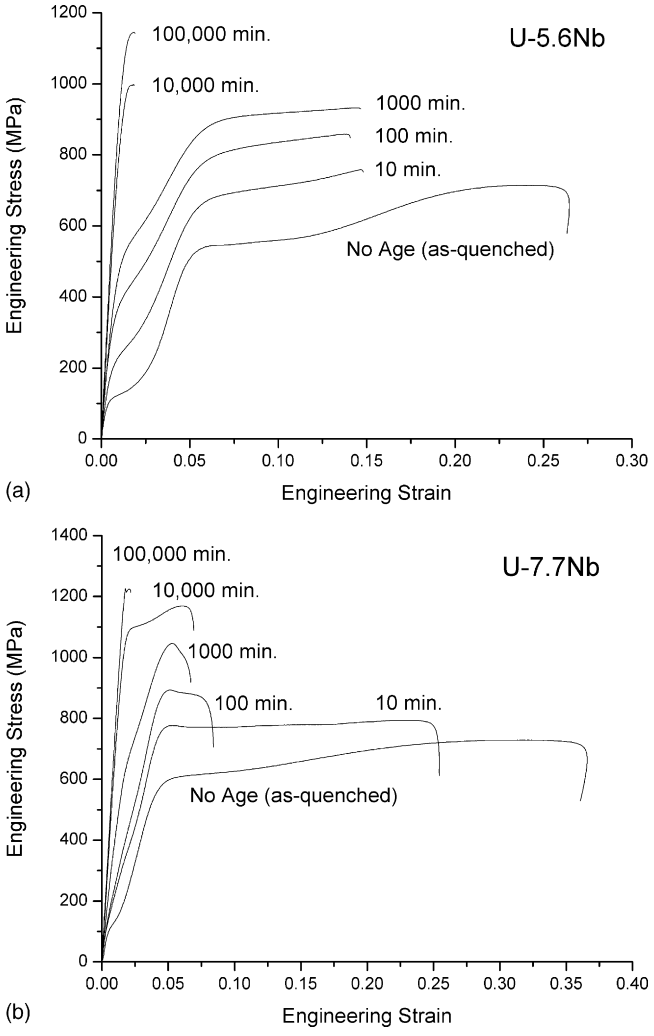

Fig. 4. Tensile stress–strain response during aging at 523 K for the times indicated for (a) U–5.6Nb and (b) U–7.7Nb.

TEM characterization efforts of these alloys in the non-overaged conditions of interest to this study failed to show unambiguous signs of classical strengthening mechanisms, namely solute clustering and/or precipitation. Even at the longest ages (just prior to peak age) the only signs of aging are roughened twin boundaries and mottled twin interiors. Fig. 7 shows the TEM results from U–7.7Nb aged for 10^5 min at 573 K. The lower magnification image (Fig. 7a) shows what appears to be the γ^0 twins from the as-transformed microstruc-

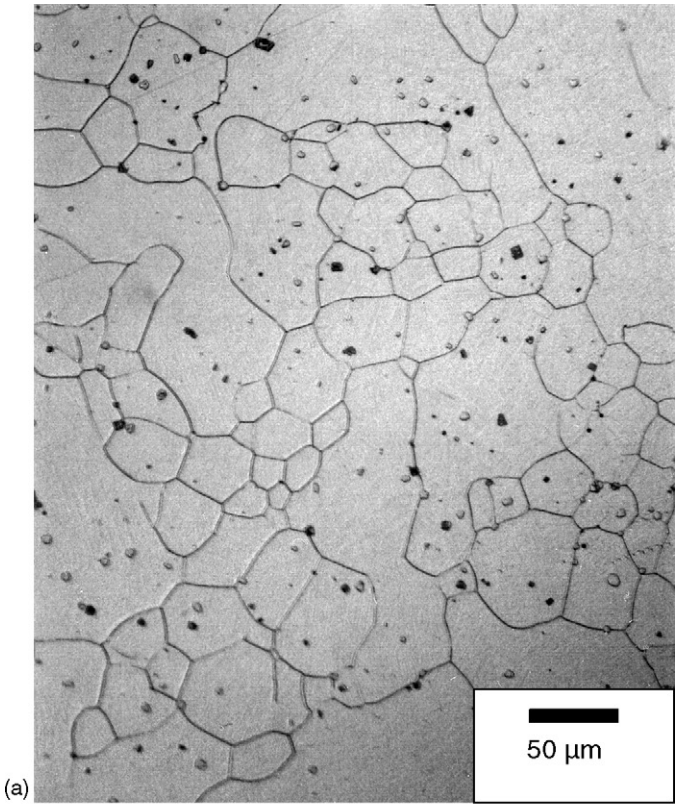

Fig. 5. Light optical micrographs of U–5.6Nb in (a) as-quenched condition and (b) after aging 100,000 min at 573 K.

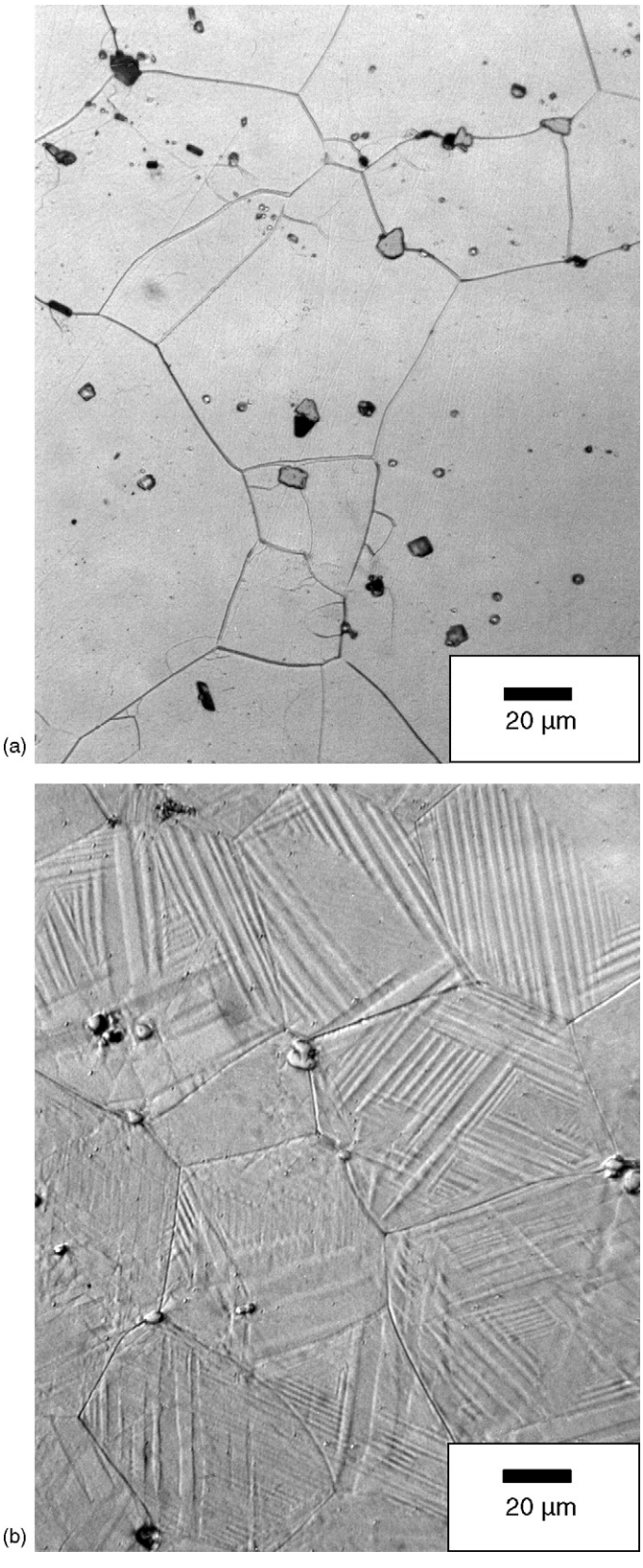

Fig. 6. Light optical micrographs of U–7.7Nb in (a) as-quenched condition and (b) after aging 1000 min at 573 K.

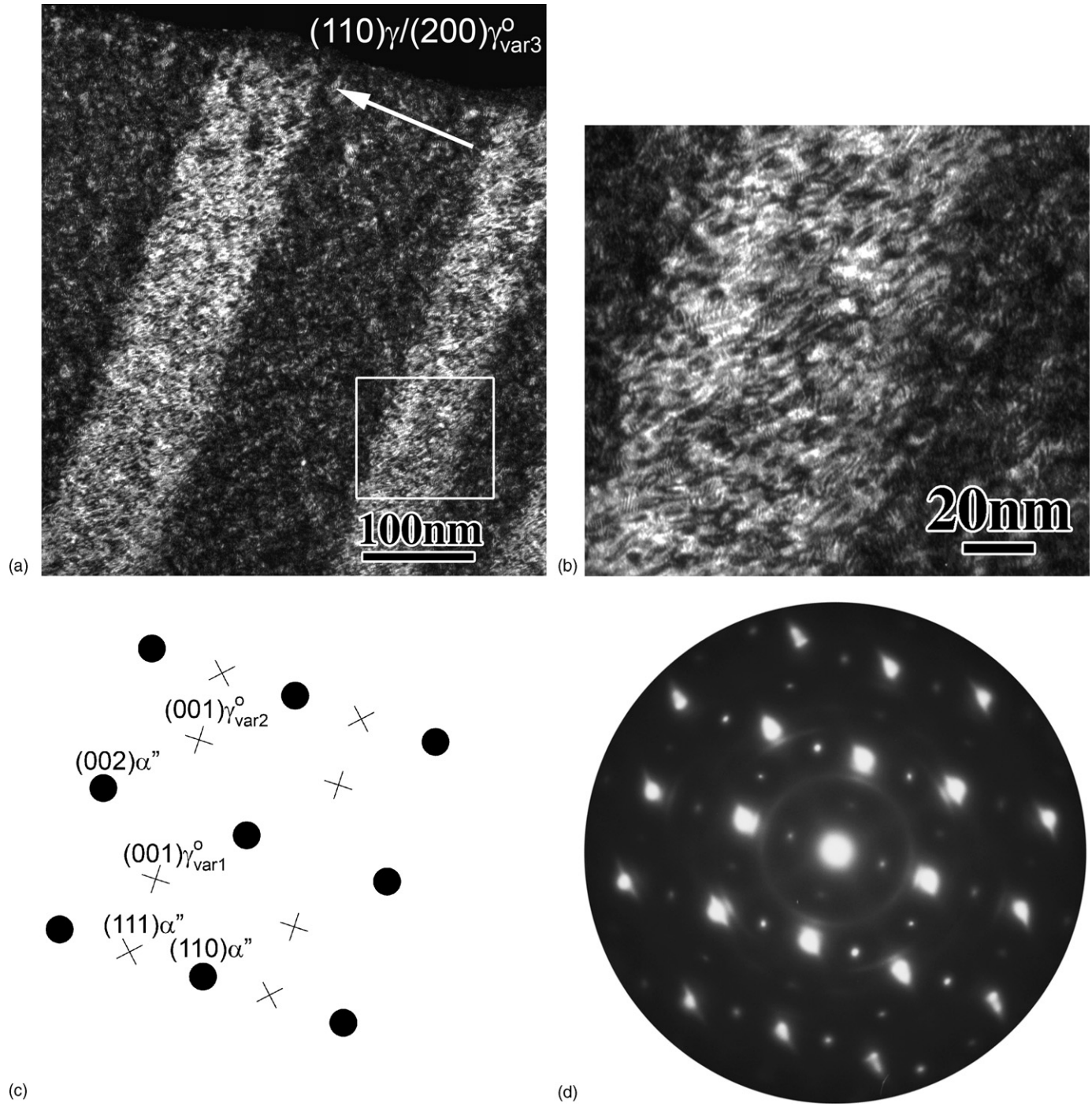

Fig. 7. (a) Dark field TEM micrograph showing the microstructure of a U–7.7Nb specimen aged for 10^5 min at 573 K. (b) A section of the micrograph in (a) at higher magnification to show the mottled structure. (c) Simulated SAD pattern showing expected positions for overlapping α'', γ^0, and γ reflections (round spots) and additional reflections expected from γ^0 (+), and α'' (×). (d) Experimental SAD pattern from a [0 0 1] γ zone axis (see text for details).

ture as well as a fine mottled microstructural feature on a scale of ~10 nm that is better defined in the higher magnification image of Fig. 7b. This structure suggests a phase separation within the γ^0 phase. Inspection of the simulated and experimental selected area diffraction (SAD) patterns in Fig. 7c and d provides insight into the nature of this separation. In the simulation, the round symbols represent reflections from the γ parent phase (as well as overlapping γ^0 and α'' reflections), the +'s represent the additional reflections associated with the γ^0 phase variants and the ×'s the extra reflections associated with one of the 12 α'' martensite variants. Note that the extra reflections in the experimental pattern are consistent with the α'' phase, not the γ^0 phase. Since the selected area aperture included both apparent γ^0 twins in the image, at least one of the three possible variants that give rise to the γ^0 superlattice reflections should appear in the experimental pattern. Similar data from other zone axes also are consistent

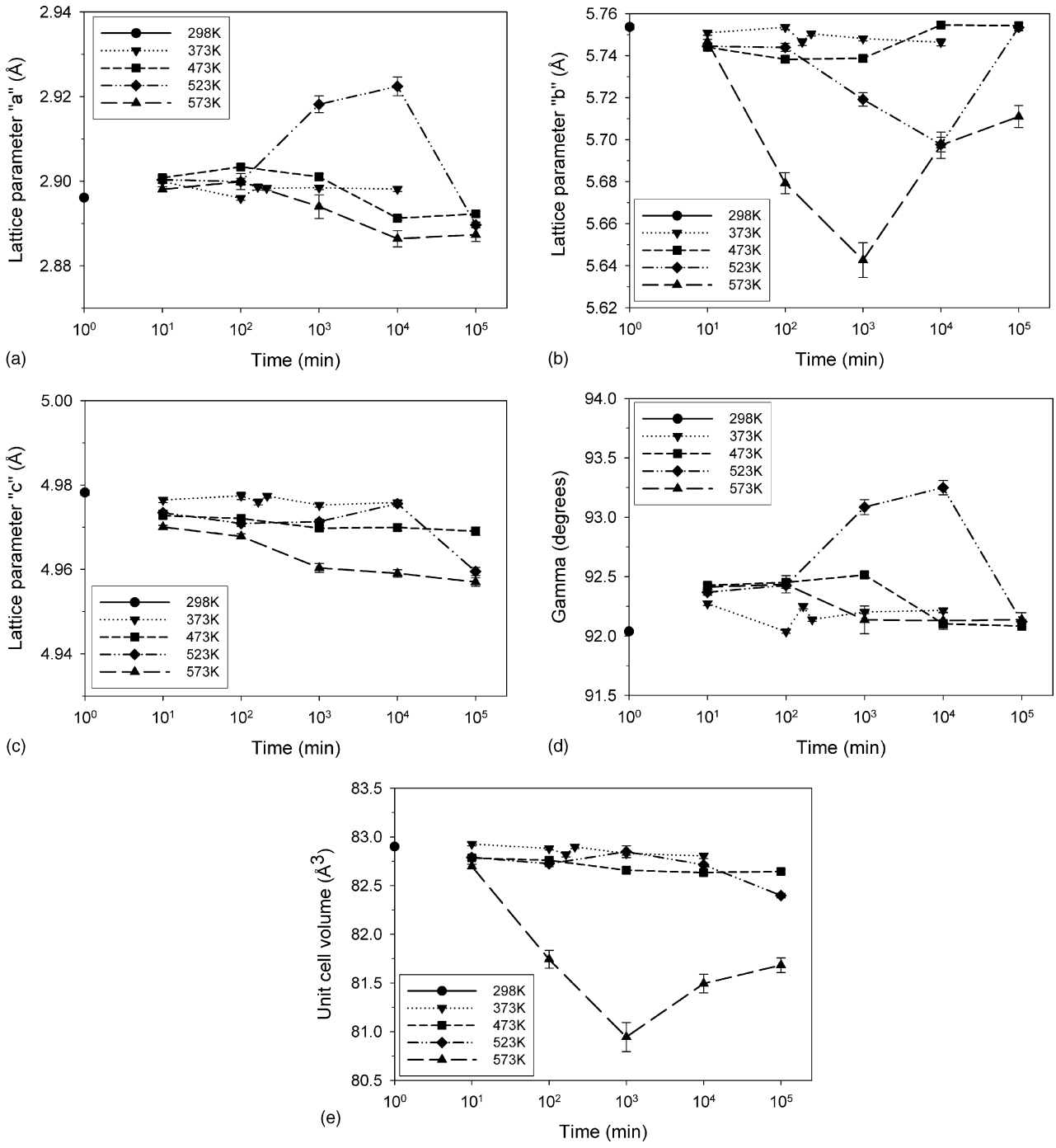

Fig. 8. Time evolution of refined lattice parameters with artificial aging time and temperature for U–5.6Nb alloy. Note that for this monoclinic structure a non-standard setting was used with γ as the oblique angle.

with the presence of a two phase mixture of γ and a partially constrained α″.

Fig. 8a–e shows variations in lattice parameters from the nominally monoclinic α″ U–5.6Nb samples. Error bars on the lattice parameters represent the uncertainty in the least-squares fitting of the data for these variables, multiplied by the slope of the normal probability plot (typically 2–2.5). At 373 K, three samples were aged for similar times (100, 165, and 215 min) and had statistically indistinguishable hardnesses. Spreads in lattice parameters for these three samples give an estimate of sample reproducibility. Stephens parameters [14] were used to model the anisotropic microstrain broadening in these samples, the March–Dollase model [15,16] was used to account for a small amount of texture, atom positions were refined but damped, and the isotropic thermal motion parameters were held fixed at realistic values. Due to correlations and imposed constraints we did not analyze trends in the resultant peak profile parameters such as microstrain, but the lattice parameters resulting from Rietveld refinements of these data show interesting behavior and should not be heavily dependent on details of peak profile

fits. In particular, note that the change in b over time at the highest temperature initially decreases, followed by a sharp increase (Fig. 8b). The data at 523 K follow this trend with a time delay. In the raw data for these temperatures (Fig. 9a and b), peak broadening can be seen with time, but this appears to be followed by sharpening at the longest times.

Lattice parameter measurements during aging in the related alloys of U–2Mo [12] and U–0.5Ti [13] showed decreasing b lattice parameter values during initial strengthening, then the trend reversed and b increased (toward the value of unalloyed α-U) during overaging reactions initiated at grain boundaries and inclusions. In those studies, the a and c lattice parameters changed relatively little during aging. Ammons [13] also cited isothermal dilatometry at 773 K in U–0.59Ti and U–0.75Ti that showed an initial volume contraction prior to the later-stage volume expansion, which is also consistent with the unit cell volume trend at 573 K in Fig. 8e. The correlation of b parameter reversal with the onset of coarse-scale overaging reactions in U–2Mo and U–0.5Ti does not hold for the present results on U–5.6Nb, as no grain-boundary or inclusion-nucleated products were observed at any time studied here, including times beyond the reversal in the b lattice parameter (Fig. 5b). The differences in overaging correlation may be attributable to subtle differences that exist between the matrix orthorhombic α′ phase in the U–2Mo and U–0.5Ti and the monoclinic α″ phase that is the matrix in U–5.6Nb. The atomic percent of solute in the bulk alloy may also play a role, as it is correlated with the magnitude of the change in the b parameter between its as-quenched and minimum values (∼0.01 Å in 0.5 wt.% Ti = 2.4 at.% Ti; ∼0.02 Å in 2 wt.% Mo = 4.8 at.% Mo; and ∼0.10 Å in 5.6 wt.% Nb = 13.2 at.% Nb).

One hypothesis that may account for the reversal behavior in U–5.6Nb involves consideration of the transition from coherent to partially coherent precipitates. As the equilibrium phase diagram dictates, precipitation of a niobium-rich γ-like phase is expected. The changes in lattice parameter trends (initially in the opposite of the anticipated direction for niobium diffusing out of solution) could reflect the difficulty of the lattice in elastically accommodating coherent niobium precipitates or clusters. The maxima/minima in the lattice parameter data may represent a loss of coherency, followed by the matrix phase becoming leaner in niobium. Further elaboration on this matter necessitates detailed TEM studies.

Data from the nominally tetragonal γ^0 phase (U–7.7Nb) in Fig. 10 proved to be more challenging to refine. Two as-quenched samples were studied; the spread in these data provide an estimate of sample reproducibility. Peak profile parameters such as microstrain were highly unstable, and prone to diverge upon refinement. Data analysis was complicated by unusually large shoulders on some of the diffraction peaks. This could be due to high strains in the sample, but also may be explained by the presence of a small amount of α″ phase, which is expected in niobium lean regions formed during aging and is consistent with the electron diffraction data from the long-aged U–7.7Nb specimen, which indicated the presence of a constrained α-like phase (Fig. 7).

The X-ray diffraction data were refined with both monoclinic and tetragonal phases present, thereby improving the appearance

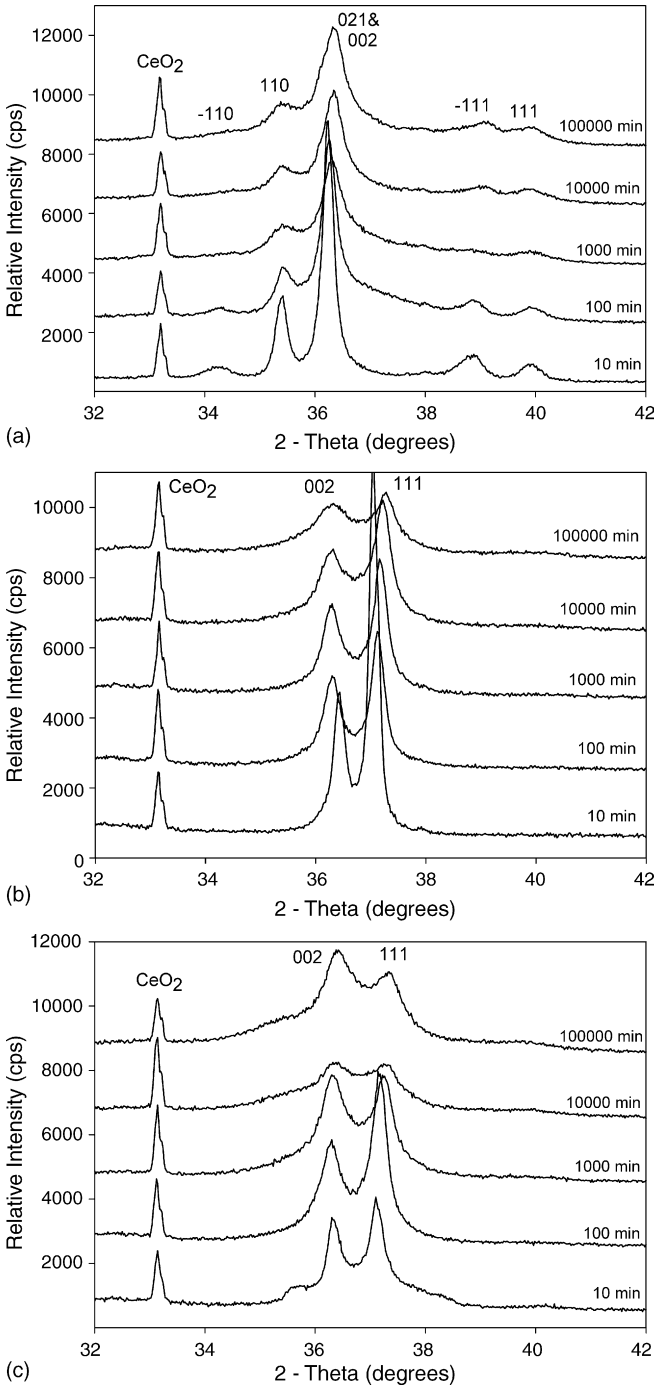

Fig. 9. Raw data at fixed composition and aging temperature for various aging times. Intensities have been staggered for easier viewing. Numbers above peaks refer to Miller indices ($h\,k\,l$): (a) U–5.6Nb, 573 K; (b) U–7.7Nb, 523 K; (c) U–7.7Nb, 573 K.

of the refinement of the data. A microstrain broadening term was also added to the refinement, but due to high correlations only the isotropic microstrain term within the simplest pseudo-Voigt profile function could be refined. Still, the isotropic microstrain for a few of the highly aged specimens had to be fixed due to a tendency for these refinements to diverge. Addition of the crystallite size broadening term to the U–7.7Nb refinements improved the fit, but usually had to be done iteratively with microstrain. This

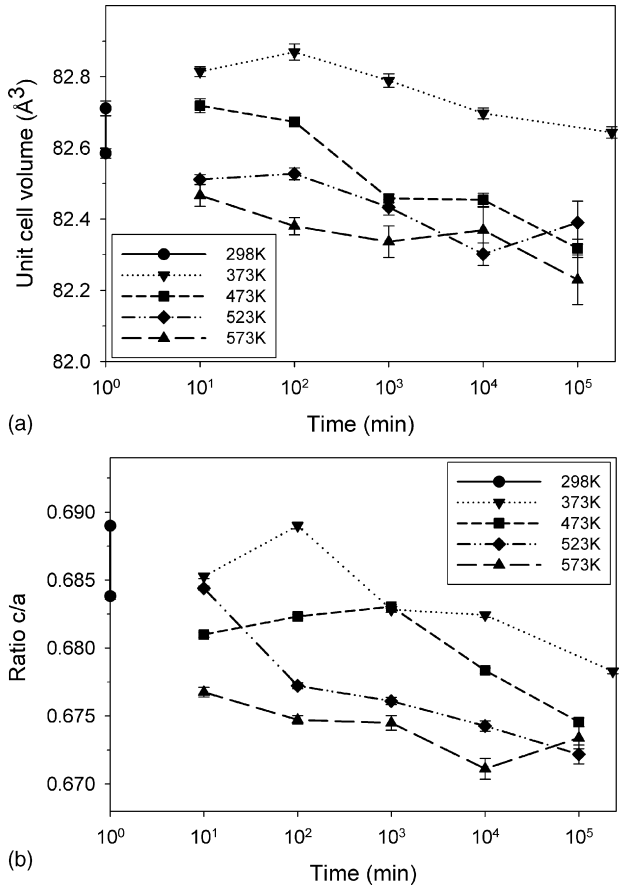

Fig. 10. Time evolution of (a) refined unit cell volume and (b) *c*/*a* ratio with artificial aging time and temperature for U–7.7Nb alloy. Note that for the system to approach the equilibrium γ phase, this *c*/*a* ratio would approach 0.707, due to the relationship of this tetragonal unit cell to the bcc γ unit cell.

is a simplistic modeling of complex peak shapes, but generally the isotropic microstrain term tended toward large but physically possible values whereas the crystallite size broadening remained relatively small. For the small amount of the α″ second phase, we were unable to refine peak profiles and isotropic thermal motion parameter adequately, and we fixed them to values observed to be realistic for less aged material. The α″ lattice parameters often had to be refined iteratively, then fixed. Weight fractions of α″ were typically less than 10%, and often around 5%. As mentioned earlier, planar defects (i.e., stacking faults and twins) may be the reason for the unusual appearance of the diffraction data. More work is needed to adequately incorporate these microstructural features in the refinements, but the lattice parameter results are not expected to change significantly. The trends visible in Fig. 10 indicate a clear decrease in unit cell volume during aging, perhaps due to more of the smaller substitutional niobium atoms in the γ^0 phase. This would lead to precipitation of an α-like phase, lean in niobium. The TEM observations of U–7.7Nb aged 573 K for 100,000 min (Fig. 7) are consistent with such a Nb redistribution process that produces Nb-lean α″- and Nb-rich matrix γ or γ^0. Changes in *c*/*a* ratio indicate a decrease in Nb content. However, this could be due to coherency strains with precipitates, as with the U–5.6Nb alloy. The *c*/*a* ratio decrease is consistent with an accommodation of the γ^0 to α″ transformation strain, thus decreasing coherency strains between the two phases.

Future work will center upon examining the role of planar defects on diffraction data and accounting for these features in Rietveld refinement. Both optical (Fig. 6b) and transmission electron microscopy (Fig. 7) show twinning is present, and as mentioned above, it is believed that planar faults may be contributing to peak profiles in the diffraction data that are difficult to accommodate within GSAS. Ultimately, an improved refined fit to the data that incorporates these microstructural details may yield valuable insights as to the behavior of the atoms within this material as it approaches equilibrium, and detailed analyses of planar defects could lead to an enhanced understanding of aging mechanisms operating in the U–Nb system. It is conceivable that improved analyses of these existing data as well as new data could change these ideas as to aging methodology, as it has been a challenging material to understand. To this end, neutron diffraction analyses, EXAFS studies, and atom probe measurements are all being performed in order to assist in explaining aging-related phenomena.

4. Conclusions

In summary, low temperature artificial aging in U–Nb alloys results in significant strengthening and ductility loss but with few signs of the aging process visible by optical or electron microscopy. X-ray diffraction is a more sensitive technique to study this aging, but large microstrains complicate X-ray data analysis. Artificial aging data from the monoclinic α″ specimens (U–5.6Nb) at high temperatures show a reversal in lattice parameter trends with time, hypothetically caused by a loss of coherency of Nb precipitates growing in a matrix that becomes progressively leaner in Nb with aging. Data from the U–7.7Nb, which appear to contain some α″ phase, show generally decreasing unit cell volumes with aging, indicating of Nb enrichment of the matrix phase. Explanations of all data are complicated by challenging Rietveld refinements, which point towards inclusion of features such as planar faults and more detailed strain modeling in future analyses.

Acknowledgements

D.R. Korzekwa, F.G. Garcia, R. McCabe, R. Trujillo, D.L. Hammon, B.L. Bingham and S.W. Quintana produced the U–Nb plate material used in this study. T. Tucker and C.J. Vigil assisted with heat treating and M.F. Lopez ran the tensile tests. Pallas Papin prepared specimens for TEM. Los Alamos National Laboratory is operated by Los Alamos National Security LLC for the U.S. Department of Energy under contract DE-AC52-06NA25396.

References

[1] T.B. Massalski (Ed.), Binary Alloy Phase Diagrams, 2nd ed., ASM, Materials Park, OH, 1990.
[2] K.H. Eckelmeyer, A.D. Romig Jr., L.J. Weirick, Metall. Trans. A 15A (1984) 1319.

[3] K. Tangri, D.K. Chaudhuri, J. Nucl. Mater. 15 (1965) 278.
[4] M. Anagnostidis, M. Colombie', H. Monti, J. Nucl. Mater. 11 (1964) 67.
[5] Donald Brown, private communication, Los Alamos National Laboratory, Los Alamos, NM, 2006.
[6] R.J. Jackson, Report RFP-862, Dow Chemical Co., Golden, CO, 1967.
[7] A.M. Kelly, D.J. Thoma, R.D. Field, P.S. Dunn, D.F. Teter, J. Nucl. Mater. 353 (2006) 158.
[8] W. Soller, Phys. Rev. 24 (1924) 158.
[9] SRM 674a, CeO_2, National Institute of Standards and Technology, U.S. Department of Commerce, Gaithersburg, MD, 1983.
[10] A.C. Larson, R.B. Von Dreele, General Structure Analysis System, Report LA-UR-86-748, Los Alamos National Laboratory, Los Alamos, NM, 1986.
[11] R.D. Field, D.J. Thoma, P.S. Dunn, D.W. Brown, C.M. Cady, Philos. Mag. A 81 (2001) 1691.
[12] K.H. Eckelmeyer, in: J.J. Burke, et al. (Eds.), Physical Metallurgy of Uranium Alloys, Brook Hill, Chestnut Hill, MA, 1976, p. 463.
[13] A.M. Ammons, in: J.J. Burke, et al. (Eds.), Physical Metallurgy of Uranium Alloys, Brook Hill, Chestnut Hill, MA, 1976, p. 511.
[14] P. Stephens, J. Appl. Cryst. 32 (1999) 281.
[15] W.A. Dollase, J. Appl. Cryst. 19 (1986) 267.
[16] A. March, Z. Kristallogr. 81 (1932) 285.